

Article

Magnesium Strengthening in 3D Printed TCP Scaffold Composites

Carmen H. Escalera ^{1,2}, Ignacio Alejandro Figueroa ^{1,*}, Mariano Casas-Luna ²,
Francisco Javier Rodríguez-Gómez ³, Cristina Piña-Barba ¹, Edgar B. Montufar ² and Ladislav Čelko ²

¹ Instituto de Investigaciones en Materiales, Universidad Nacional Autónoma de México, Ciudad Universitaria, Coyoacán, Ciudad de Mexico 04510, Mexico; elena-carmen@comunidad.unam.mx (C.H.E.)

² Central European Institute of Technology, Brno University of Technology, 61200 Brno, Czech Republic

³ Facultad de Química, Universidad Nacional Autónoma de México, Ciudad Universitaria, Coyoacán, Ciudad de Mexico 04510, Mexico

* Correspondence: iafigueroa@unam.mx

Abstract: This study reports the production of a Mg/15%β-tricalcium phosphate Ca₃(PO₄)₂ composite by combining direct ink writing for the β-TCP preform and liquid infiltration technique to obtain a continuous metal matrix composite. The influence of the volume fraction of β-TCP and the in situ reaction between ceramic and metal on the microstructure and mechanical properties were investigated in detail. The β-TCP preform was uniformly distributed in the matrix, forming a continuous three-dimensional (3D) network. The obtained composite was characterized by means of relative density (He pycnometry), X-ray diffractometry (XRD), scanning electron microscopy (SEM), and electron spectroscopy (EDX). The results suggested that a highly densified composite was processed. Three phases were identified as products generated by an exothermic reaction (Mg₂Ca, CaO, and MgO); based on this, the chemical reaction mechanism for MgO formation was proposed. The compression and hardness tests showed that the Mg/15%β-tricalcium phosphate Ca₃(PO₄)₂ composite significantly improved its mechanical properties, i.e., 27% and 15% higher than pure Mg in compressive strength and yield strength, respectively. This behavior was attributed to the high densification of the resulting composite, strong chemical interfacial bonding, phase dispersion hardening (in situ phase formation), and the geometry and continuity of the reinforcement. These provided good load transfer from the Mg matrix to the reinforcement and contributed as strengthening mechanisms. The results reported in this investigation can help to design Mg/calcium phosphate continuous composites for biomedical applications.

Keywords: metal matrix composites (MMCs); 3-dimensional reinforcement; mechanical properties; liquid metal infiltration; in situ formed particles



Citation: Escalera, C.H.; Figueroa, I.A.; Casas-Luna, M.; Rodríguez-Gómez, F.J.; Piña-Barba, C.; Montufar, E.B.; Čelko, L. Magnesium Strengthening in 3D Printed TCP Scaffold Composites. *J. Compos. Sci.* **2023**, *7*, 467. <https://doi.org/10.3390/jcs7110467>

Academic Editor: Xiang Xu

Received: 27 September 2023

Revised: 20 October 2023

Accepted: 25 October 2023

Published: 9 November 2023



Copyright: © 2023 by the authors. Licensee MDPI, Basel, Switzerland. This article is an open access article distributed under the terms and conditions of the Creative Commons Attribution (CC BY) license (<https://creativecommons.org/licenses/by/4.0/>).

1. Introduction

Magnesium (Mg)-based metal matrix composites (MMCs) have been developed to fulfill different demands as lightweight and high-strength materials in the aerospace, automotive, defense, biomedical, and other industries [1]. This has led to new research on different ways to produce this kind of material. Metal matrix composites often combine two or more pre-existing constituents, i.e., metallic matrix material and ceramic reinforcement. A metal matrix composite usually has better properties than the individual constituents (i.e., high specific modulus, strength, and thermal stability); thus, it can be considered a novel material [1]. The processes commonly used to produce this type of material include powder metallurgy, diffusion bonding, liquid phase sintering, and stir casting [2]. One of the disadvantages of these processes is that the reinforcement is usually discontinuous. In addition, the reinforcement is generally less than 10 wt.% since, with a higher amount, there is a risk of agglomeration, favoring the formation of pores and defects that could reduce the mechanical properties. At the same time, the significant advantage of those processes

is the relatively short production time and the control of chemical reactions between the reinforcement and metal [2].

The liquid-state processes have been extensively employed in the production of MMCs. However, the liquid metal infiltration technique is one of the most important techniques used for producing different MMCs by the free selection of different ceramic preforms and the metal matrix [3,4]. These processes are characterized by close interfacial bonding, making a strong adhesion. The dispersed material is incorporated into a molten metal matrix, which later undergoes solidification. In MMCs, the matrix material plays an important role, providing support for the dispersed phase and stabilizing the composite structure [5]. In addition, the quality of the dispersed phase-matrix interfacial bonding determines the mechanical properties of the composite [6]. Compared to solid-state methods, liquid-state processes are relatively simple and cost-effective. These processes also permit the formation of dense matrices and near-net-shaped components, even in complex geometries, at a considerably fast production rate [7–10]. Ceramic reinforcement materials for MMCs can be classified into continuous reinforcement and discontinuous reinforcement (short fibers, whiskers, and particles) [11]. Nowadays, continuous reinforcement structures can be additively manufactured using 3D printing techniques. 3D printing is a series of advanced manufacturing technologies used to fabricate parts in a discrete point-by-point, line-by-line, and layer-by-layer additive fashion from 3D CAD models [12]. In addition, 3D printing and its technology have solved previous processing limitations, i.e., fabricating complex structures and achieving highly complicated geometries with interconnected pores [13]. The control of the strut's diameter and length impacts the mechanical properties of the produced component [14]. Direct ink writing (DIW) or robocasting is one of the most popular material extrusion technologies [14]. DIW has a lower requirement for ink material preparation than other deposition techniques, and the quantity of material feeding volume per nozzle is much higher than in other techniques [12]. In this process, a powder ink based on the material of interest (i.e., β -TCP ($\text{Ca}_3(\text{PO}_4)_2$)) is prepared by incorporating a binder material, mainly a polymer. Afterward, the ink is placed into a syringe and loaded into the 3D printing device, which controls the displacement of the syringe to print the desired pattern previously designed in CAD. It is worth mentioning that the infiltration of a ceramic preform with liquid Mg, especially in calcium-based preforms, represents a technical challenge since several factors affect the quality of manufactured MMCs; one of the most important is the poor wettability between the solid ceramic scaffold and the molten metal [15]. The liquid metal infiltration process resolves this problem. However, due to the fact that it is not a spontaneous process, it requires the application of an external force (pressure) to overcome the surface tension between the ceramic and the liquid metal so that the liquid metal can penetrate the interstices of the preform, without damaging the reinforcement structure. Only a few works have explored the combination of additive manufacturing to produce MMCs, mostly direct ink writing, with different forms of infiltrations, i.e., metal/metal, polymer/polymer, or ceramic/metal composites [16–21].

Multiple parameters have been considered to achieve the desired mechanical properties; for instance, preform geometry, preform fraction, distribution of the continuous components and the strength of the interfacial bond [16,22–26]. For the latter, a route to ensure better bounding between the particle and matrix is the in situ decomposition reaction. A reaction between Mg and ceramic reinforcement during casting can significantly affect the interfacial bond and, thus, the mechanical properties [27], even though some studies have tried to avoid this reaction and its products [28,29]. In other cases, however, this helps the in situ production of a dispersed phase within the matrix, carried out by a chemical reaction that is typically exothermic [30]. Generally, the in situ process provides a more homogeneous distribution of the dispersed phase particles. This route also tends to ensure better particle-matrix bonding, allowing the introduction of a large volume fraction and a small-sized dispersed material. A disadvantage of in situ processing of MMCs is that the kinetics of the process determine the particle size and shape during the nucleation and growth process. The most used reinforcements are silicon carbide (SiC), aluminum oxide

(Al₂O₃), carbon (C), graphene, etc. [31]. The in situ processing of composite materials is cost-effective and scalable; however, for commercial applications, the chemical reactions are unpredictable, and insufficient knowledge of the processes must be addressed [32–35]. Studies have yet to be carried out on the mechanism responsible for the in situ formation of distinct phases due to the interaction of CaP, specifically β -TCP and Mg and its effect on their mechanical properties. Therefore, further analysis is required to propose this material for biomedical device applications.

Based on the above, in this study, a Mg/15% β -TCP composite was developed by combining two processing techniques: direct ink writing and the liquid pressure infiltration route. The first helps control the ceramic reinforcement distribution, and the final produces a continuous composite material. The 15% β -TCP was chosen as an intermediate volume fraction considering studies previously reported since it is the minimum geometrically optimal vol.% provided by the 3D printer. On the other hand, pure Mg was chosen to facilitate the understanding of the reaction mechanism between the matrix and the ceramic preform to determine the role of the individual reinforcements (ceramic, intermetallic, and oxides) on the mechanical properties.

2. Materials and Methods

The continuous Mg/ β -TCP composite fabrication consisted of two steps: a) production of the porous β -TCP preform by DIW, and b) liquid infiltration of the β -TCP scaffold with molten Mg.

2.1. Production of β -TCP Preform

The ceramic ink for additive manufacturing was prepared by homogeneously mixing commercial β -TCP Ca₃(PO₄)₂ powder (VWR Chemicals) and 40% *w/w* Pluronic F-127 (Sigma Aldrich, Darmstadt, Germany) solution in distilled water, i.e., 6 g of Pluronic solution per gram of β -TCP powder [26]. Then, the ink was loaded into a commercial syringe (Optimum[®], syringe barrels, Nordson EFD) and placed in the DIW system (Pastecaster, Fundació CIM, Barcelona, Spain). Next, the preforms were robocast using 410 μ m tapered dispensing tips (SmoothFlow Tapered Tips, Nordson EFD, Westlake, OH, USA) at 8 mm·s⁻¹. Cylindrical preforms were built following an orthogonal grid pattern of parallel filaments (Figure 1). Subsequently, the preforms were dried at room temperature for 24 h and sintered in a furnace (LH30/13, LAS) at 1100 °C for 9 h with a heating rate of 2.5 °C/min. The β -TCP preforms were 9 mm in diameter, with 11 filaments per layer.

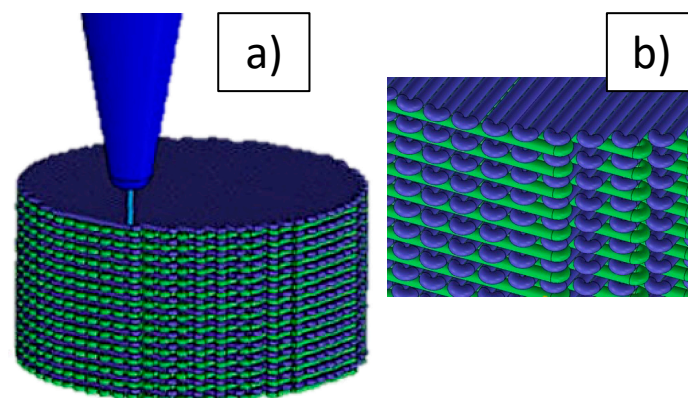


Figure 1. A schematic of the DIW process: (a) assembly preform, (b) orthogonal grid pattern.

2.2. Liquid Metal Infiltration

The Mg/ β -TCP composite was prepared by infiltrating the β -TCP scaffold with molten Mg (99.95 % Sigma Aldrich) using pressurized Ar gas [1], as shown in Figure 2. In the process, an Mg ingot was placed on top of the β -TCP preform (parallel to the printed direction) in a stainless-steel crucible coated with boron nitride. The chamber was

evacuated to remove the air from the system (Figure 2a); once a vacuum of 10^{-2} KPa was reached, Ar was introduced into the crucible chamber to produce a protective atmosphere to avoid Mg oxidation (Figure 2b). The crucible was then placed into a furnace (Carbolite®) preheated at 760 °C. Consequently, an Ar pressure of 50 KPa was applied on the melt surface to force Mg to fill the interstices of the preform (Figure 2c). Finally, after 20 min, the crucible was removed from the furnace to cool down to room temperature by placing it on a copper block, allowing directional solidification (Figure 2d). The composite produced was machined into cylinders of 9 mm in length and 6 mm in diameter.

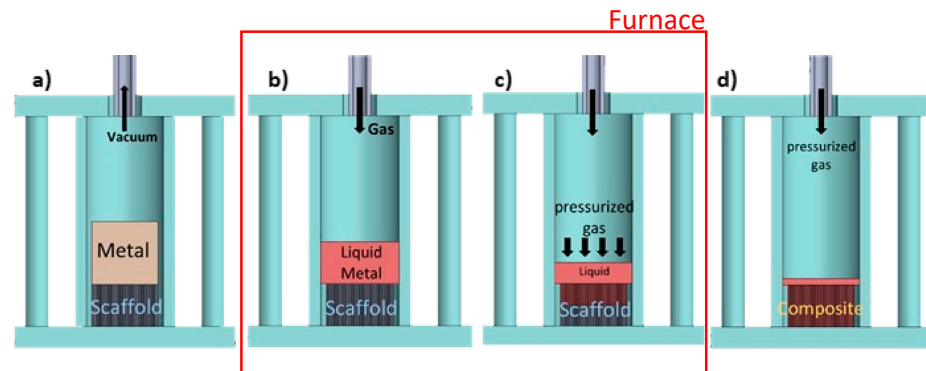


Figure 2. Stainless steel crucible design and layout for the infiltration process: (a) layout of the system before the infiltration (protective atmosphere), (b) melting process, (c) liquid metal infiltration process, and (d) composite cooling.

For the microstructure observation and phase composition characterization, the composites were longitudinally cut and polished with SiC abrasive paper and diamond suspension down to a 1 μm finish. Then, X-ray diffraction (XRD, Rigaku, SmartLab 3 kW, Japan) was employed to determine the crystalline phases using the HighScore + software (PANalytical, Almelo, The Netherlands) and ICDD PDF 2 and ICSD 2012 databases. The scans were performed using Cu K- α ($\lambda = 0.154$ nm) with a current of 30 mA and a voltage of 40 kV in Bragg Brentano geometry between 20° and 80° with a scanning speed of 2° min^{-1} .

The microstructure was observed through scanning electron microscopy (SEM; TESCAN, Lyra 3, Brno, Czech Republic) equipped with a dispersive energy X-ray (EDS) spectroscope (INCA, Oxford Instruments, Oxford, UK). Representative images were obtained using an electron beam voltage of 5 kV. Elemental EDS analyses were performed on the identified phases to determine the element distribution and the possible inter-phase reaction. SEM-image analysis was employed to measure the diameter and separation of the filaments in the preforms. In addition, the preforms and composites were coated with a nanometric carbon layer to prevent charging during the SEM observations. Finally, the preform and the Mg/ β -TCP composite volume were measured using a He pycnometer (Quantachrome Ultrapyc 1200e, Graz, Austria). From the obtained results, the experimental density, and the effective porosity of the preform, Φ , were calculated according to $\Phi = \frac{V_S - V_B}{V_S}$, where V_S is the volume of the sample and V_B is the volume occupied by the β -TCP (solid volume). Furthermore, the results were compared with an estimated theoretical density using the rule of mixtures, i.e., the ceramic fraction, the metal matrix fraction, and the theoretical density values of pure Mg and β -TCP (1.738 g cm^{-3} and 3.05 g cm^{-3}), respectively [36].

Compression tests were performed using a universal mechanical testing machine (TIRA GmbH, test model 2850s, Schalkau, Germany) at a strain rate of $4.1 \times 10^{-4} \text{ s}^{-1}$. The specimens were machined to have a cylindrical geometry of 6 mm in diameter and 9 mm in length to meet the requirements for the ASTM E9 standard [37]. Five identical samples were used for the compression test (parallel to the printed direction) to generate the stress-strain curves (the averages are presented with standard deviations). Vickers hardness was measured using a micro-hardness tester (Shimadzu HVM-G2) with a load of 0.98 N for 15 s.

The specimen surfaces were carefully polished before testing, and 10 measurements were carried out for statistical purposes.

3. Results

3.1. Chemical and Microstructural Characterization of β -TCP Preform

Figure 3a,b shows an interconnected preform with an orthogonal β -TCP pattern. The diameter of the preform was 6.8 ± 0.14 mm, the diameter of the filaments was 305 ± 15 μ m, and the in-layer separation between them was 206 ± 40 μ m, producing a linear shrinkage in the preform of 26%. The surface of the β -TCP (Figure 3c) consisted of equiaxed polyhedral grains and some intergranular microporosity with 48 ± 8 μ m in size. The crystalline composition was corroborated to identify the corresponding crystallographic phase, matching the β -TCP phase (ICSD: 006191) (Figure 4).

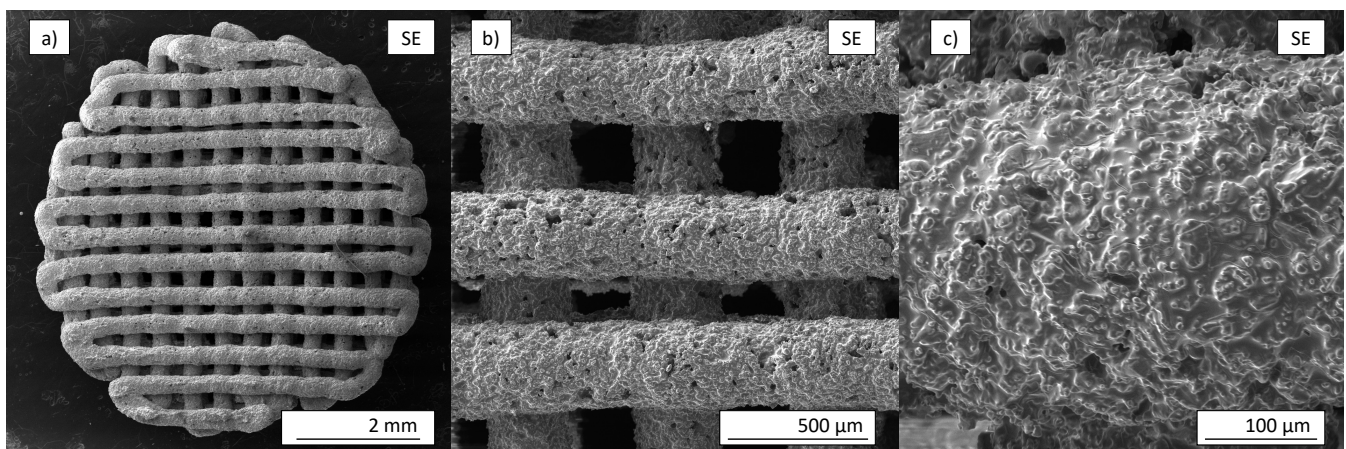


Figure 3. SEM images of 3D-periodic β -TCP preform: (a) top view, (b) cross-section, and (c) high-magnification of a filament.

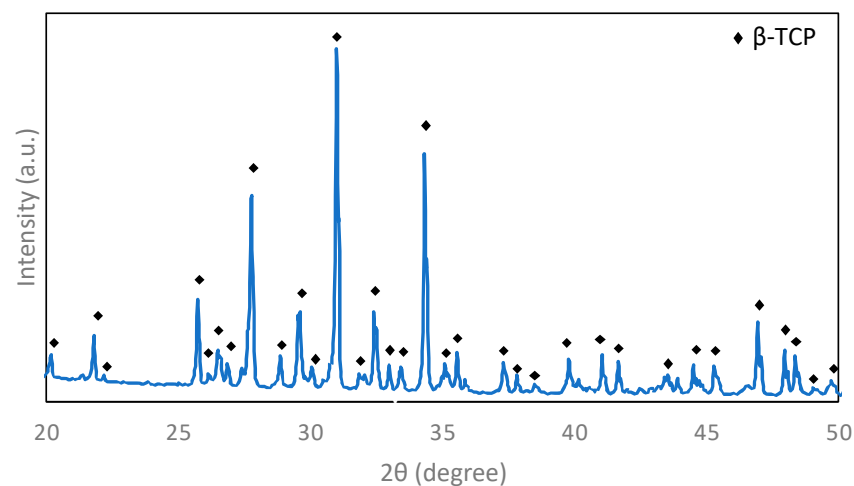


Figure 4. X-ray diffraction pattern for the consolidated β -TCP preform.

The preform resulting porosity (Φ) was $84.46 \pm 0.08\%$ (Table 1). The final structure, with a homogenous spacing between the filaments, produced an open pore network, providing a large contact surface and excellent structural integrity.

Table 1. Theoretical and experimental densities of the separated elements and resulting Mg/ β -TCP composite.

Sample	Density [g/cm ³]		Φ [%]
	Theoretical	Experimental	
β -TCP	3.05	3.0349 \pm 0.0008	84.46 \pm 0.08
Mg	1.74	1.7354 \pm 0.0005	-
Mg/ β -TCP	1.94 *	2.02 \pm 0.08	1.94 \pm 0.01

* Calculated using the rule of mixtures for composite materials.

3.2. Chemical and Microstructural Characterization of the Mg/ β -TCP Composite

The resulting Mg/ β -TCP composite was successfully obtained, as shown in Figure 5a, with a compact structure, i.e., the liquid metal filled the pores, producing a two-phase structure, where each phase was continuous and self-connected through the composite material. In terms of densities, for the β -TCP, the theoretical (3.05 g/cm³) and experimental (3.0349 \pm 0.0008 g/cm³) densities were rather similar; however, the experimental density was slightly lower (Table 1), as expected. Similar behavior was also observed for the Mg. On the other hand, the composite material showed an experimental density slightly higher than the theoretical. This could be attributed to the formation of other phases, i.e., Mg₂Ca, MgO, and CaO, that were not considered in the rule of mixtures calculation (Table 1).

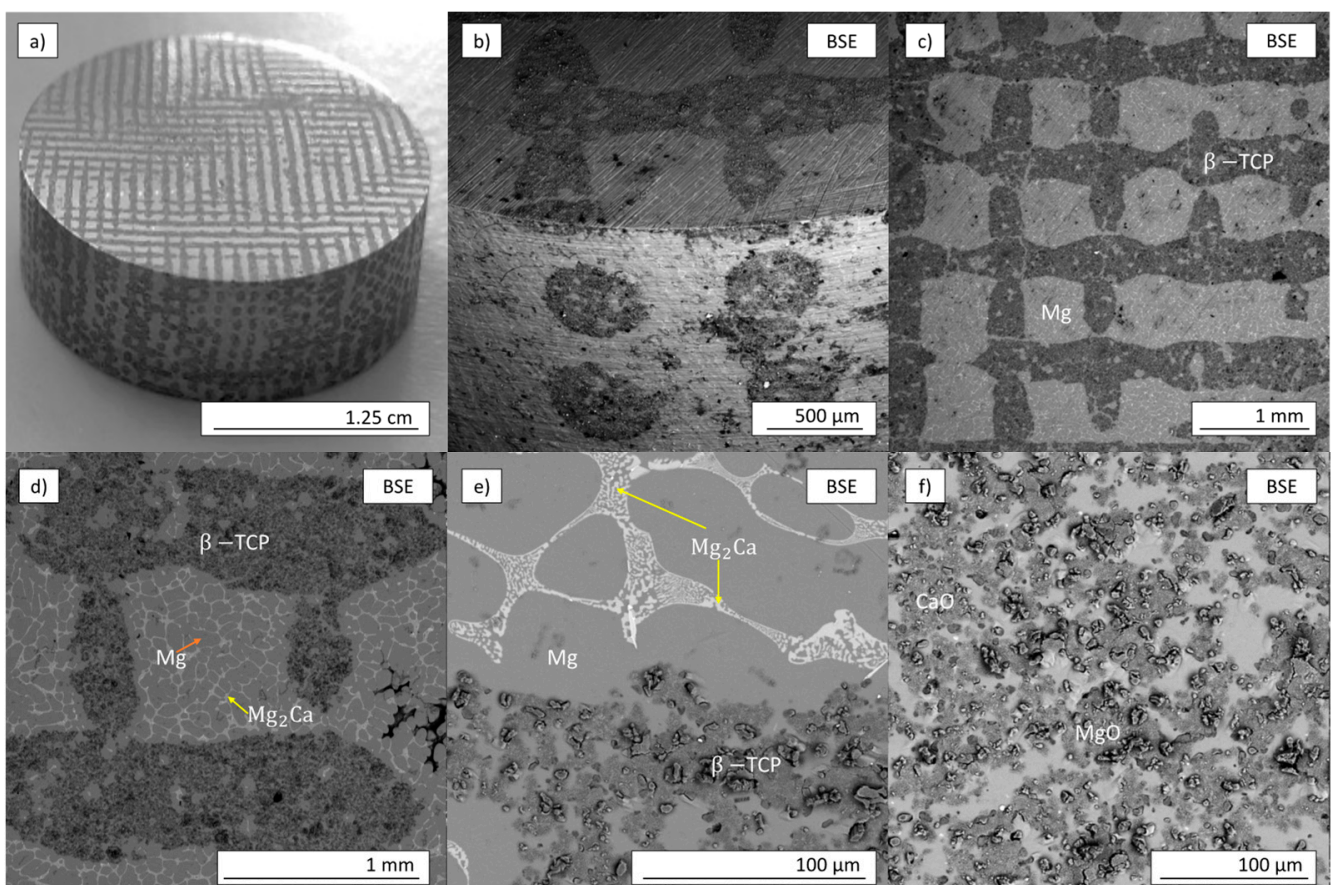


Figure 5. (a) Macroscopic appearance of a representative interpenetrating Mg/ β -TCP composite. SEM micrograph of Mg/ β -TCP composite: (b) edge view, (c) overview, (d) low magnification of β -TCP pattern and Mg matrix, (e) high magnification of the interface region, and (f) high magnification of the β -TCP filament (ceramic area).

The SEM microstructural analysis showed that Mg penetrates the porosity and intergranular porosity observed within the β -TCP filaments (Figure 5c,d), resulting in a highly compact Mg/ β -TCP composite structure. Furthermore, the EDS analysis was employed for the punctual chemical analyses of the resulting phases (Figure 6). From the EDS analyses (Table 2), in zone (a), oxygen (O), carbon (C), and Mg were detected, being correlated with the Mg matrix. In zone (b), O, C, calcium (Ca), and Mg were located at the grain boundaries, corresponding to the intermetallic Mg_2Ca . Finally, in zones (c) and (d), C, phosphorous (P), Ca, O, and Mg were observed in the filaments, attributed to the β -TCP, MgO, and CaO phases (Figures 5f and 6). The XRD patterns confirmed the presence of the intermetallic Mg_2Ca and the Mg and MgO phases. No peak of CaO was observed in Figure 7, probably because the amount produced was not within the XRD detectable range.

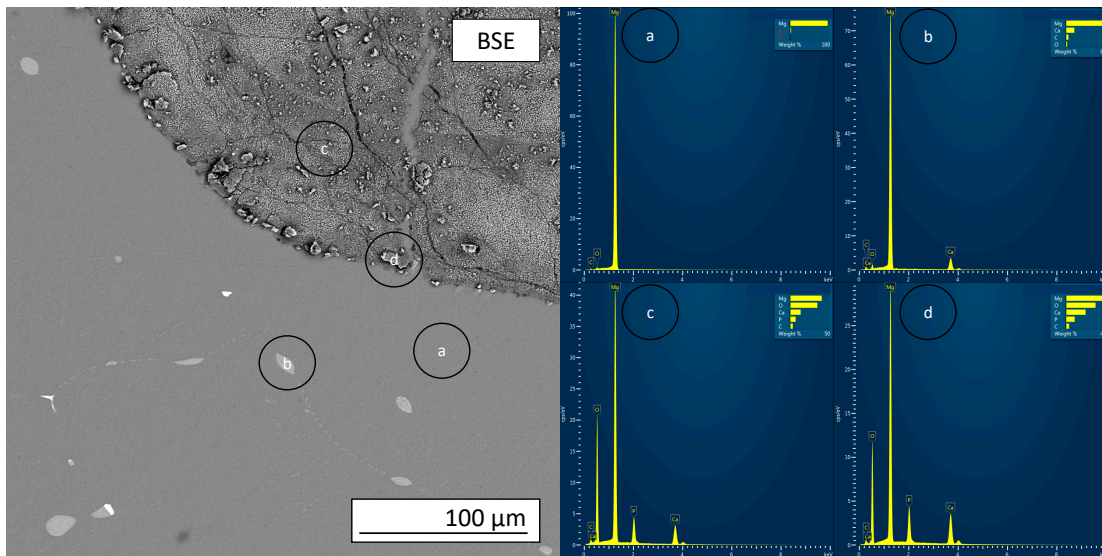


Figure 6. Representative image of the interface and elemental analysis EDS showing the distribution of the elements C, Ca, O, P, and Mg in four different Mg/ β -TCP composite regions.

Table 2. Elemental analysis of four different Mg/ β -TCP composite regions.

Zone	C %	O %	Mg %	Ca %	P %
a	11.00	1.50	87.50	-	-
b	10.96	4.31	74.22	10.51	-
c	6.20	42.01	34.22	11.16	6.52
d	6.94	46.17	35.18	7.2	4.96

Values are in at. %. Zones a, b, c and d are located in Figure 6.

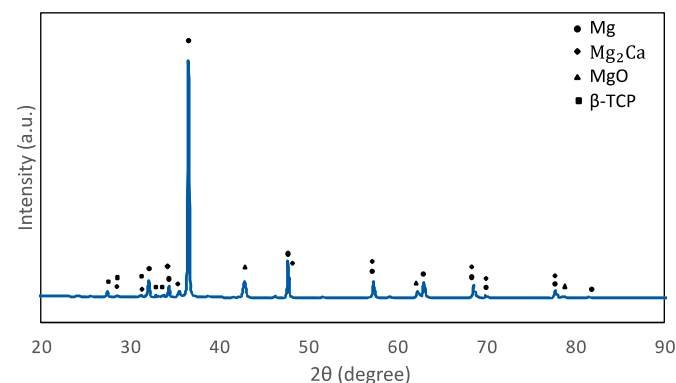


Figure 7. X-ray diffraction patterns of interpenetrating phase Mg/ β -TCP composite.

3.3. Mechanical Properties of Interpenetrating Mg/ β -TCP Composite

The stress–strain curves of the materials studied in the compression test are shown in Figure 8. The β -TCP preform showed compressive strength with two orders of magnitude lower than that of Mg, showing a brittle behavior. The effect of Mg infiltration on compressive behavior was evident. The average compressive strength of the Mg/ β -TCP composite (220 ± 5 MPa) was almost 180 times higher than that of the original porous preform β -TCP (1.2 ± 0.05 MPa), approximately 27% higher than the bulk Mg (160 ± 5 MPa). On the other hand, the yield strength value for the Mg/ β -TCP composite was 150 ± 2.2 MPa, almost 15% higher than the pure Mg (131 ± 7.6 MPa). The fracture surface of the composites displayed a brittle failure of the metallic phase. Moreover, the propagation path of the crack produced within the ceramic phase was restricted and deflected along the ceramic–metal interface, producing an interfacial debonding. Micro-Vickers hardness tests were carried out in two areas, i.e., the Mg-matrix and the β -TCP filaments. The hardness values were 58 ± 4.6 HV and 112.63 ± 10.13 HV, respectively.

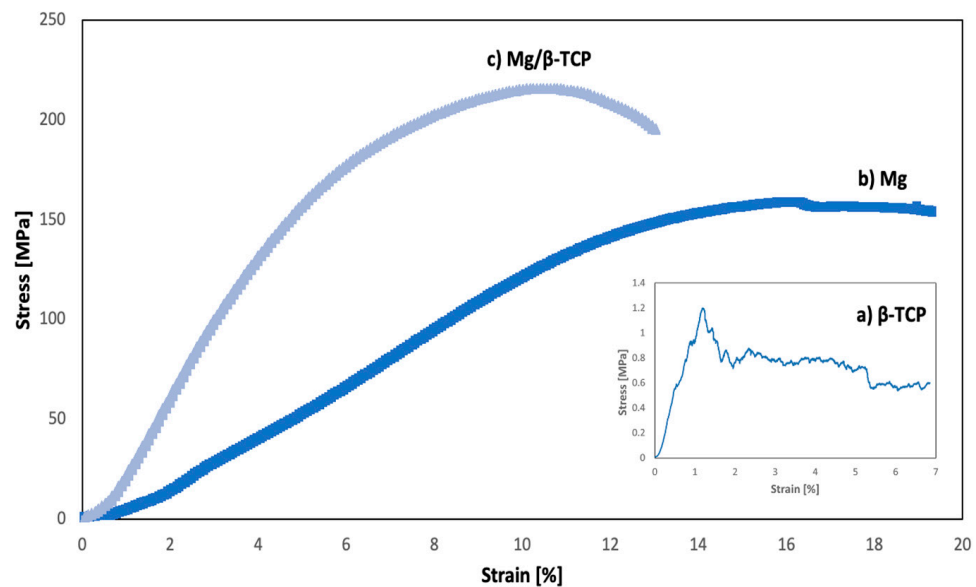


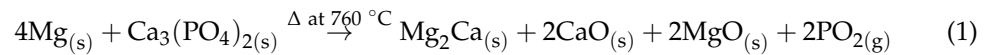
Figure 8. Compressive stress–strain curves of (a) β -TCP, (b) pure Mg, and (c) Mg/ β -TCP composite.

4. Discussion

Due to the high efficiency achieved by the liquid infiltration process ($\sim 98\%$) (Figure 5b), the production technique reported in this work could be proposed for manufacturing metal–ceramic composites with a homogeneously topological relationship between the components. This process reduced interfacial energy, improving the wettability between the preform and the liquid Mg, creating a highly compact composite. This was achieved by controlling the Ar gas pressure, promoting the Mg infiltration while avoiding the β -TCP structural damage. In other words, the preform could be designed with special requirements (i.e., chemically, topologically, etc.), retaining its original shape once the composite has reached its final form. One of the most significant advantages was that the infiltration time could control the metal matrix and ceramic reinforcement (Mg and β -TCP) chemical reaction.

The results also indicate that the in situ reaction between the Mg and β -TCP filaments produced the additional Mg_2Ca , CaO, and MgO phases. Please bear in mind that the reduction and oxidation of other calcium phosphate (CaP) products (e.g., hydroxyapatite) have been observed even during solid-state processes such as spark plasma sintering or pressure-less infiltration [27–29,38]. Narita et al. [27] reported that the reaction around 530°C was exothermic, with an abrupt mass loss due to the decomposition of the β -TCP, resulting in the possible release of phosphorous oxide gas (PO_2). However, the mechanism through which Mg reduces CaPs has been described by exclusively considering

the formation of MgO [17,27,39,40] without contemplating the possible formation of other phases, such as Mg₂Ca, CaO, etc., as reported in this study. The proposed mechanism for decomposing the β-TCP involves the following steps: (a) the liquid Mg enters directly in contact with the preform β-TCP filaments, and (b) the liquid Mg reduces the β-TCP. This can be represented by the following reaction:



The formation of CaO in the composite could be attributed to the phosphate reduction. However, the proposed reaction does not generate Ca since the decomposition temperature of the CaO is above 1000 °C [41]. Nevertheless, it has been reported that the intermetallic Mg₂Ca is formed during the heating and infiltration process [26], considering that Mg can dissolve up to 1.34 wt.% Ca (at 789.5 K) [42,43]. Therefore, if the amount of Ca²⁺ reaches the solubility limit in Mg, the nucleation and growth of Mg₂Ca is thermodynamically favored, producing an additional phase. Then, after β-TCP reduction, the intermetallic Mg₂Ca phase (5.1 at.%) is formed and segregated during the solidification at the grain boundaries. This causes the high densification of the Mg/β-TCP composite (Table 1). A MgO layer was not identified between the Mg matrix and β-TCP scaffold interface; only MgO particles were observed in the β-TCP filament (Figure 5f). In this study, the formation of allotropes or compounds such as calcium phosphide (Ca₃P₂), magnesium phosphide (Mg₃P₂), or phosphine (PH₃) could be possible [44]. However, they could be produced in the first or intermediate part of the reaction; therefore, they are not represented in the proposed chemical reaction (1).

On the other hand, the phosphorous (P) found in the struts (Figure 6c,d and Table 2) indicated that the reaction does not entirely degrade the β-TCP, confirming that the amount of particle reinforcement can be controlled by adjusting the time taken for the infiltration process. The findings of the densification and in situ reaction potentially facilitate designing not only the Mg/β-TCP composite with MgO as a reaction product [27] but also other reaction products such as metal oxides (CaO) or intermetallic phases (Mg₂Ca).

The abovementioned changes in the microstructure did affect the mechanical properties. The difference in the yield strength between the pure Mg and the composite could be attributed to the in situ reaction between the Mg and β-TCP, which produced a highly densified composite without voids or shrinkage that could affect the mechanical behavior. Besides, a strong interfacial bond between the matrix and reinforcement is important since it improves shear strength, as the load is effectively transferred from the matrix to the β-TCP preform [45]. Recently, it has been reported that the failure of composite materials is associated with particle cracking and the formation of voids in the matrix within particle clusters [45]. Another factor that needs to be considered is the phase dispersion hardening in the in situ formed Mg₂Ca phase. This phase will interact with dislocations and even grain boundary movement, increasing the strength of the composite material [46,47]. The interconnected distribution of the β-TCP structure eliminates stress concentrators, like fibers that tend to act as stress concentrators. Coarser ceramic particles will have a higher probability of containing defects that initiate the fracture. In a 3D arrangement, the fibers or struts are continuous, reducing the stress concentrator points.

Based on the above, the improved mechanical properties of the Mg/β-TCP composite reported in this work give way to the possibility of tailoring the reaction mechanism by topologically designing the solid pattern of the preform so the metal matrix could react with the reinforcement, producing a microstructure that generates the mechanical properties required for a possible biomedical application. For instance, for cortical bones, the highest UCS reported is 283 MPa [48] and for the Mg/β-TCP composite is 220 MPa, which lays within the range required for bone fixation [48].

5. Conclusions

A highly compact Mg/15% β -TCP composite was successfully developed by combining two innovative techniques, i.e., 3D printing and liquid infiltration process. The reinforcement, β -TCP, was fabricated using the direct ink writing technique, generating a topological design with an interconnected structure. In the infiltration part, a chemical reaction occurred due to the high reactivity of Mg, leading to surface decomposition of the β -TCP preform, forming MgO and CaO precipitates in the struts. The decomposition of the β -TCP also formed a homogeneously segregated intermetallic Mg₂Ca at the Mg grain boundaries. A high densification was achieved, reducing pores or voids (down to 1%) in the composite, producing a strong interfacial bond between the Mg and ceramic reinforcement. The produced microstructure improved the mechanical properties, developing a lightweight and high-strength composite. The chemical reaction control of Mg and β -TCP during infiltration would reduce intermetallic phase segregation at grain boundaries. With the results presented in this study, the production of continuous Mg/CaP composites with optimal mechanical properties could be employed as biodegradable metal composites for hard tissue scaffolds. The methodology proposed in this work can be extrapolated to develop other reactive metal–ceramic systems for aerospace, automotive, defense, and other industries.

Author Contributions: C.H.E.: Formal analysis, Investigation, Data curation, Writing—original draft, Visualization. I.A.F.: Methodology, Formal analysis, Investigation, Funding acquisition, Supervision, Writing—initial draft. M.C.-L.: Investigation, Data curation, Writing. F.J.R.-G.: Methodology, Formal analysis, Investigation. C.P.-B.: Methodology, Resources, Writing—review & editing. E.B.M.: Methodology, Formal analysis, Investigation, Funding acquisition, Writing. L.Č.: Conceptualization, Methodology, Supervision, Funding acquisition, Writing—review & editing. All authors have read and agreed to the published version of the manuscript.

Funding: Part of this work was supported by the project MatProcessing-4-Med (5SA14634), funded by the European Union’s Horizon 2020 research and innovation program under the Marie Skłodowska-Curie; co-financed by the South Moravian Region under grant agreement 665860; and from DGAPA-PAPIIT UNAM “IN102422” for funding the project.

Data Availability Statement: The data supporting this study’s findings are available within the article.

Acknowledgments: I.A.F. would like to acknowledge C. Flores, G. A. Lara-Rodriguez, C. Ramos, A. Tejada, O. Novelo-Peralta, L. Bazán, A. Bobadilla, F. Garcia, E. Hernandez-Mecinas, E. Reyes, R. Reyes, C. González are also acknowledged for their technical support. “Por mi raza hablará el espíritu”.

Conflicts of Interest: The authors declare no conflict of interest.

References

1. Etemadi, R.; Wang, B.; Pillai, K.; Niroumand, B.; Omrani, E.; Rohatgi, P. Pressure infiltration processes to synthesize metal matrix composites—A review of metal matrix composites, the technology and process simulation. *Mater. Manuf. Process.* **2018**, *33*, 1261–1290. [[CrossRef](#)]
2. Kaczmar, J.W.; Pietrzak, K.; Wlosinski, W. The production and application of metal matrix composite materials. *J. Mater. Process Technol.* **2000**, *106*, 58–67. [[CrossRef](#)]
3. Orboluv, I.; Németh, A.; Dobránszky, J. Composite production by pressure infiltration. *Mater. Sci. Forum* **2008**, *589*, 137–142.
4. Blucher, J.; Narusawa, U.; Katsumata, M.; Nemeth, A. Continuous manufacturing of fiber-reinforced metal matrix composite wires—Technology and product characteristics. *Compos. Part A Appl. Sci. Manuf.* **2001**, *32*, 1759–1766. [[CrossRef](#)]
5. Kainer, K.U. *Metal Matrix Composites: Custom-Made Materials for Automotive and Aerospace Engineering*; John Wiley & Sons: Weinheim, Germany, 2006.
6. Balasubramanian, M. *Composite Materials and Processing*, 1st ed.; CRC Press: Boca Raton, FL, USA, 2013. [[CrossRef](#)]
7. Suresh, S.; Mortensen, A. *Fundamentals of Metal-Matrix Composites*, 1st ed.; Elsevier Science: Amsterdam, The Netherlands, 2013.
8. Efzan, E.; Nordin, S.S.; Al Bakri, A.M.M. Fabrication method of aluminum matrix composite (AMCs): A review. *Key Eng. Mater.* **2016**, *700*, 102–110.
9. Natarajan, N.; Krishnaraj, V.; Davim, J.P. *Metal Matrix Composites: Synthesis, Wear Characteristics, Machinability Study of MMC Brake Drum*; Springer: Berlin/Heidelberg, Germany, 2014.
10. Ceschini, L.; Dahle, A.; Gupta, M.; Jarfors, A.E.; Jayalakshmi, S.; Morris, A.; Singh, R.A. *Aluminum And Magnesium Metal Matrix Nanocomposites*; Springer: Singapore, 2017; pp. 19–20.

11. Jayalakshmi, S.; Gupta, M. *Metallic Amorphous Alloy Reinforcements in Light Metal Matrices*; Springer: New York, NY, USA, 2015.
12. Chen, Z.; Li, Z.; Li, J.; Lao, C.; Fu, Y.; Liu, C.; Li, Y.; Wang, P.; He, Y. 3D printing of ceramics: A review. *J. Eur. Ceram. Soc.* **2019**, *39*, 661–687. [[CrossRef](#)]
13. Zhang, F.; Li, Z.; Xu, M.; Wang, S.; Li, N.; Yang, J. A review of 3D printed porous ceramics. *J. Eur. Ceram. Soc.* **2022**, *42*, 3351–3373. [[CrossRef](#)]
14. Nichols, R.W. *Advanced Materials by Design: New Structural Materials Technologies*; DIANE Publishing: Washington, DC, USA, 1988.
15. Sobczak, N.; Singh, M.; Asthana, R. High-temperature wettability measurements in metal/ceramic systems—Some methodological issues. *Curr. Opin. Solid. State. Mater. Sci.* **2005**, *9*, 241–253. [[CrossRef](#)]
16. San Marchi, C.; Kouzeli, M.; Rao, R.; Lewis, J.; Dunand, D. Alumina–aluminum interpenetrating-phase composites with three-dimensional periodic architecture. *Scr. Mater.* **2003**, *49*, 861–866. [[CrossRef](#)]
17. Chang, H.; Higginson, R.; Binner, J. Microstructure and property characterisation of 3-3 Al(Mg)/Al₂O₃ interpenetrating composites produced by a pressureless infiltration technique. *J. Mater. Sci.* **2010**, *45*, 662–668. [[CrossRef](#)]
18. Stevanovic, S.; Philippe, C. Improvement of Mechanical Properties of 3d Printed Hydroxyapatite Scaffolds by Polymeric Infiltration. *Bioceram. Dev. Appl.* **2013**, *3*, 10–12. [[CrossRef](#)]
19. Zhang, S.; Zhang, X.; Zhao, C.; Li, J.; Song, Y.; Xie, C.; Tao, H.; Zhang, Y.; He, Y.; Jiang, Y.; et al. Research on an Mg–Zn alloy as a degradable biomaterial. *Acta. Biomater.* **2010**, *6*, 626–640. [[CrossRef](#)] [[PubMed](#)]
20. Liu, D.; Huang, Y.; Prangnell, P. Microstructure and performance of a biodegradable Mg-1Ca-2Zn-1TCP composite fabricated by combined solidification and deformation processing. *Mater. Lett.* **2012**, *82*, 7–9. [[CrossRef](#)]
21. Wang, X.; Li, J.; Xie, M.; Qu, L.; Zhang, P.; Li, X. Structure, mechanical property and corrosion behaviors of (HA+β-TCP)/Mg-5Sn composite with interpenetrating networks. *Mater. Sci. Eng. C* **2015**, *56*, 386–392. [[CrossRef](#)]
22. Seleznev, M.; Shulz, B.; Cornie, J.; Zhang, S.; Sachs, E.; Serdy, J.; Cima, M. Development of Novel tool-less net-shape pressure infiltration casting technology for manufacturing metal matrix composites. In *State of the Art in Cast Metal Matrix Composites in the Next Millenium [SiC]: Proceedings of a Symposium*; Metallurgical Society of AIME: New York, NY, USA, 2000; pp. 81–88.
23. Wang, X.; Zhang, P.; Dong, L.; Ma, X.; Li, J.; Zheng, Y. Microstructure and characteristics of interpenetrating β-TCP/Mg-Zn-Mn composite fabricated by suction casting. *Mater. Design.* **2014**, *54*, 995–1001. [[CrossRef](#)]
24. Wang, X.; Nie, Q.; Ma, X.; Fan, J.; Yan, T.; Li, X. Microstructure and properties of co-continuous (β-TCP+MgO)/Zn-Mg composite fabricated by suction exsorption for biomedical applications. *Trans. Nonferrous Met. Soc. China* **2017**, *27*, 1996–2006. [[CrossRef](#)]
25. Son, J.; Lee, W.; Park, Y.; Park, I. Fabrication and thermal expansion behavior of a magnesium-matrix composite with a high content of reinforcing SiC particles. *Mech. Compos. Mater.* **2011**, *47*, 427–434. [[CrossRef](#)]
26. Casas-Luna, M.; Tkachenko, S.; Horynová, M.; Klakurková, L.; Gejdos, P.; Diaz-de-la-Torre, S.; Celko, L.; Kaiser, J.; Montufar, E.B. Interpenetrated Magnesium–Tricalcium Phosphate Composite: Manufacture, Characterization and In vitro Degradation Test. *Acta. Metall. Sin.* **2017**, *30*, 319–327. [[CrossRef](#)]
27. Narita, K.; Konayashi, E.; Sato, T. Sintering Behavior and Mechanical Properties of Magnesium/β-Tricalcium Phosphate Composites Sintered by Spark Plasma Sintering. *Mater. Trans.* **2016**, *57*, 1620–1627. [[CrossRef](#)]
28. Zhou, T.; De Hosson, J. Reactive wetting of liquid metals on ceramic substrates. *Acta. Mater.* **1996**, *44*, 421–426. [[CrossRef](#)]
29. Nath, S.; Tripathi, R.; Basu, B. Understanding phase stability, microstructure development and biocompatibility in calcium phosphate -titania composites, synthesized from hydroxyapatite and titanium powder mixture. *Mater. Sci. Eng. C* **2009**, *29*, 97–107. [[CrossRef](#)]
30. Reddy, B.; Das, K.; Das, S. A review on the synthesis of in situ aluminum-based composites by thermal, mechanical and mechanical–thermal activation of chemical reactions. *J. Mater. Sci.* **2007**, *42*, 9366–9378. [[CrossRef](#)]
31. Jo, I.; Jeon, S.; Lee, E.; Cho, S.; Lee, H. Phase formation and interfacial phenomena of the in-situ combustion reaction of Al-Ti-C in TiC/Mg composites. *Mater. Trans.* **2015**, *56*, 661–664. [[CrossRef](#)]
32. Ajayan, P.M.; Schadler, L.S.; Braun, P.V. *Nanocomposite Science and Technology*; John Wiley & Sons: New York, NY, USA, 2006.
33. Yi, X.S.; Du, S.; Zhang, L. *Composite Materials Engineering, Different Types of Composite Materials*; Springer: Berlin/Heidelberg, Germany, 2018; Volume 12.
34. Trinh, S.N.; Sastry, S.; Processing And Properties Of Metal Matrix Composites. Mechanical Engineering and Materials Science Independent Study, 10. 2016. Available online: <https://openscholarship.wustl.edu/mems500/10/> (accessed on 1 August 2023).
35. Ceschini, L.; Montanari, R. *Advances in Metal Matrix Composites*; Trans Tech Publications Ltd.: Stafa-Zurich, Switzerland, 2011; p. 170.
36. Carrodeguas, R.G.; De Aza, S. α-Tricalcium phosphate: Synthesis, properties and biomedical applications. *Acta. Biomater.* **2011**, *7*, 3536–3546. [[CrossRef](#)]
37. ASTM E9-89a; Standard Test Methods of Compression Testing of Metallic Materials at Room Temperature (Withdrawn 2009). ASTM International: West Conshohocken, PA, USA, 2000.
38. Mondal, D.; Sarkar, S.; Oh, I.; Lee, B. Comparative Study of Microstructures and Material Properties in the Vacuum and Spark Plasma Sintered Tri-Calcium Phosphate Composites. *Mater. Trans.* **2011**, *52*, 1436–1442. [[CrossRef](#)]
39. Gu, X.; Zhou, W.; Zheng, Y.; Dong, L.; Xi, Y.; Chai, D. Microstructure, mechanical property, bio-corrosion and cytotoxicity evaluations of Mg/HA composites. *Mater. Sci. Eng. C* **2010**, *30*, 827–832. [[CrossRef](#)]

40. Casas-Luna, M.; Montufar, E.B.; Díaz-de-la-Torre, S.; Mendez-García, J.C.; Vištejnová, L.; Brínek, A.; Daňhel, A.; Dvořák, K.; Kaiser, J.; Čelko, L. Degradable magnesium-hydroxyapatite interpenetrating phase composites processed by current assisted metal infiltration in additive-manufactured porous preforms. *J. Magnes. Alloys* **2022**, *10*, 3641–3656. [[CrossRef](#)]
41. Wiese, B. The Effect of CaO on Magnesium and Magnesium Calcium Alloys. Ph.D. Thesis, Technische Universität Clausthal, Clausthal-Zellerfeld, Germany, 2006.
42. Dorozhkin, S. Calcium orthophosphates. *Biomatter* **2011**, *1*, 121–164. [[CrossRef](#)]
43. Li, Z.; Gu, X.; Lou, S.; Zheng, Y. The development of binary Mg–Ca alloys for use as biodegradable materials within bone. *Biomatter* **2008**, *29*, 1329–1344. [[CrossRef](#)]
44. Stüpp, C.A.; Szakács, G.; Mendis, C.L.; Gensch, F.; Müller, S.; Feyerabend, F.; Hotza, D.; Fredel, M.C.; Hort, N. Powder metallurgical synthesis of biodegradable Mg-hydroxyapatite composites for biomedical applications. In *Magnesium Technology*; Trans Tech Publications Ltd.: Stafa-Zurich, Switzerland, 2015; pp. 425–429. [[CrossRef](#)]
45. Lloyd, D.J. Particle reinforced aluminium and magnesium matrix composites. *Int. Mater. Rev.* **1994**, *39*, 1–23. [[CrossRef](#)]
46. Sharma, A.; Fujii, H.; Paul, J. Influence of Reinforcement Incorporation Approach on Mechanical and Tribological Properties of AA6061-CNT Nanocomposite Fabricated via FSP. *J. Manuf. Process.* **2020**, *59*, 604–620. [[CrossRef](#)]
47. Kwon, H.; Leparoux, M. Hot Extruded Carbon Nanotube Reinforced Aluminum Matrix Composite Materials. *Nanotechnol.* **2012**, *23*, 415701. [[CrossRef](#)] [[PubMed](#)]
48. Yusop, A.H.; Bakir, A.A.; Shaharom, N.A.; Abdul Kadir, M.R.; Hermawan, H. Porous biodegradable metals for hard tissue scaffolds: A review. *Int. J. Biomater.* **2012**, *2012*, 641430. [[CrossRef](#)] [[PubMed](#)]

Disclaimer/Publisher’s Note: The statements, opinions and data contained in all publications are solely those of the individual author(s) and contributor(s) and not of MDPI and/or the editor(s). MDPI and/or the editor(s) disclaim responsibility for any injury to people or property resulting from any ideas, methods, instructions or products referred to in the content.